PCCP

RSC Publishing

PAPER

View Article Online
View Journal | View Issue

An improved AMBER force field for α,α-dialkylated peptides: intrinsic and solvent-induced conformational preferences of model systems

Cite this: *Phys. Chem. Chem. Phys.*, 2013, **15**, 17395

Sonja Grubišić,*[ab] Giuseppe Brancato[ac] and Vincenzo Barone[ac]

α,α-Dialkylated amino acid residues have acquired considerable importance as effective means for introducing backbone conformation constraints in synthetic peptides. The prototype of such a class of residues, namely Aib (α-aminoisobutyric acid), appears to play a dominant role in determining the preferred conformations of host proteins. We have recently introduced into the standard AMBER force field some new parameters, fitted against high-level quantum mechanical (QM) data, for simulating peptides containing α,α-dialkylated residues with cyclic side chains, such as TOAC (TOAC, 2,2,6,6-tetramethylpiperidine-1-oxyl-4-amino-4-carboxylic acid) and Ac_6c (Ac_6c = 1-aminocyclohexaneacetic acid). Here, we show that in order to accurately reproduce the observed conformational geometries and structural fluctuations of linear α,α-dialkylated peptides based on Aib, further improvements of the non-bonding and side chain torsion potential parameters have to be considered, due to the expected larger structural flexibility of linear residues with respect to cyclic ones. To this end, we present an extended set of parameters, which have been optimized by fitting the energies of multiple conformations of the Aib dipeptide analogue to corresponding QM calculations that properly account for dispersion interactions (B3LYP-D3). The quality, transferability and size-consistency of the proposed force field have been assessed both by considering a series of poly-Aib peptides, modeled at the same QM level, and by performing molecular dynamics simulations in solvents with high and low polarity. As a result, the present parameters allow one to reproduce with good reliability the available QM and experimental data, thus representing a notable improvement over current force field especially in the description of the α/3_{10}-helix conformational equilibria of α,α-dialkylated peptides with linear and cyclic side chains.

Received 28th June 2013,
Accepted 7th August 2013

DOI: 10.1039/c3cp52721b

www.rsc.org/pccp

1. Introduction

Recent interest in α,α-dialkylated amino acids has been stimulated by the widespread occurrence of these residues in a large number of microbial peptide antibiotics, which may form transmembrane ion channels, and by their possible applications as biologically active peptides.[1–5] The most studied member of this class of amino acids is α-aminoisobutyric acid (Aib). It is well known that Aib may have a dramatic effect on peptide secondary structures since the rotations about the N–Cα (φ) and Cα–C (ψ) bonds of such an amino acid are quite restricted. In fact, the presence of two geminal methyl groups at Cα in Aib forces the folding of the peptide backbone chain into 3_{10}/α-helical regions ($\varphi \cong \pm 60 \pm 70$ degrees, $\psi \cong \pm 20 \pm 30$ degrees) of the peptide conformational map. Early studies on alamethicin crystal structure showed that this Aib-containing peptide adopts a mixture of 3_{10} and α-helical structures in the solid state.[6] Since 1980, a number of researchers, including Balaram's and Toniolo's groups, have performed extensive investigations on Aib peptide structures.[7–10] These studies have shown that Aib containing peptides can adopt α, 3_{10} or α/3_{10}-helical structures depending on peptide length, relative number of Aib residues and solvent apolarity.[8,11] It has been reported that the minimal length for a peptide to form an α-helix corresponds to seven residues, whereas no chain length thresholds were observed for 3_{10}-helix formation. Peptides with more than eight residues are more likely to adopt an α-helix than a 3_{10}-helix, if the content of Aib does not exceed 50%. However, with few exceptions, all Aib homopeptides adopt the 3_{10} helix conformation in the solid state.[11–13] In a previous quantum mechanical study, it has been shown that the 3_{10}-helix is the preferred conformation for an infinite Aib homopolymer *in vacuo*,[14] in agreement with IR data for Aib polymers in the solid state.[15–17] Moreover, it has been found that solvent polarity also affects the conformational preference of Aib rich peptides.[18–22] In peptides where the α/3_{10}-helix equilibrium does exist, solvents

[a] *Scuola Normale Superiore, Piazza dei Cavalieri 7, I-56126 Pisa, Italy*
[b] *Center for Chemistry, IHTM, University of Belgrade, Njegoševa 12, P.O. Box 815, 11001 Belgrade, Serbia. E-mail: grubisic@chem.bg.ac.rs*
[c] *Istituto Nazionale di Fisica Nucleare, Largo Pontecorvo 3, I-56100 Pisa, Italy*

with high polarity usually favor the α-helix formation, while the 3_{10}-helix is often found in low polarity solvents.

From a computational point of view, the comparison of results achieved by different force field (FF) based methods still provides unclear and controversial insights into conformational preferences of Aib polypeptides. One of the most common drawbacks of the available FFs for modeling natural and non-natural amino acids is their "intrinsic preference" for some conformational states (*e.g.*, α-helix), irrespective of the number of residues, nature of substituents at the Cα, and environmental effects.[23–26] An accurate description of the conformational landscape of biological systems is crucial for the study of their properties, and the prediction of peptide structures is, therefore, of great importance in life sciences, though quite challenging in practice. As a matter of fact, secondary and tertiary structures of proteins, as well as their functions, are largely determined by relatively weak nonbonding interactions such as hydrogen bonds and van der Waals forces. Although electrostatic contributions are often dominant over other interactions, a proper treatment of dispersion interactions is necessary to obtain accurate energetics. For this purpose, methods based on density functional theory (DFT) such as the DFT-D3 functionals, purposely crafted to encompass long-range forces, through empirical dispersion corrections are generally reliable in accounting for nonbonding interactions.[27] On the other hand, molecular mechanics (MM) and molecular dynamics (MD) are useful for revealing dynamics and structures of macromolecules thereby elucidating biological functions. The parameters of most FFs have been derived incrementally, that is, building on previous work by adding support for different chemical moieties in a sequential fashion. As an example, the AMBER force field has been recently extended by our group to allow simulations of nitroxide spin labels derived from cyclic α,α-dialkylated peptides.[28,29] The force-field parameterization of nitroxides was carried out to include specific structural features that are often present along side the paramagnetic center, *e.g.*, in α-amino acid nitroxides. This required the development of a force-field for the description of peptide bonds of strongly helicogenic residues with significant steric restrictions. Since nitroxides are used in condensed phases, and especially in aqueous solutions, a detailed description of medium- and long-range intermolecular effects, such as electrostatic, van der Waals and hydrogen bond interactions, is required too. The resulting FF has been employed in the integrated computational characterization of the role of structural, environmental and dynamic effects in tuning the hyperfine and gyromagnetic tensors of nitroxide spin probes, with results that are quite comparable with their experimental counterparts.[28] However, in the case of peptides based on non-cyclic residues, like Aib, due to specific intramolecular non-bonding interactions through the methyl groups, molecular dynamics results gave only qualitative agreement with experimental data.[29] This suggested that further refinement of the current AMBER force field was necessary for an accurate conformational sampling. Note that despite the ongoing developments of polarizable force fields, also by our group,[30] that account for often significant polarization effects of biomolecules, here we have focused on extensions of the AMBER force field, as a follow-up study of our previous work,[29] due to its large popularity and widespread use.

Aib is structurally similar to alanine except for an additional methyl group attached to the alpha-carbon. The dialkylation at the alpha-carbon gives rise to a significant steric hindrance, which is responsible for the helical preference of Aib. Here, we are interested in providing a reliable force field able to accurately describe the role that steric hindrance plays in governing helical structures and flexibility of Aib based peptides. To this end, we considered homopeptides of different length, such as Ac-$(Aib)_n$-NMe (Ac, acetyl; NMe, methylamino) with n = 1–33, and performed comparative MM and QM calculations of the relative stability between α and 3_{10}-helical conformations, in order to test systematically the effect of peptide length. Solvent effects have been also considered by performing simulations in gas phase, aqueous solution, and chloroform solution. In addition, we generalized the force field to be used for both cyclic and acyclic α,α-dialkylated peptides, showing that modifications related to Aib do not affect significantly the results for cyclic systems reported previously,[29] and actually improve the conformational landscape of Aib.

The paper is organized as follows: the computational methodology is presented in Section 2. First, the new parametrization of the Aib methyl group is discussed, with particular emphasis on the vdW interactions. Then, we provide some details about the MD simulations and the calculations of the geometrical observables evaluated along the MD trajectories. Section 3 contains our results and corresponding discussion. Here, the energetics of dipeptides with linear and cyclic side chains is examined carefully. The conformational dynamics of Aib tetra- and heptapeptides is also analyzed and compared with available experimental data. Concluding remarks are given in Section 4.

2. Methods

2.1. Force field parametrization

The atom types and structures of all the α,α-dialkylated dipeptide analogues Ac-X-NMe considered in the present study (namely X = Aib, Ac_6c, and TOAC) are reported in Fig. 1, together with those of the alanine dipeptide analogue. Force field parameters of Aib were derived by fitting towards QM computations on various conformers of Ac-Aib-NMe performed with the Gaussian09 package,[31] employing the SNST basis set[32] and the hybrid B3LYP functional augmented by empirical dispersion contributions (B3LYP-D3[27]). As a matter of fact, a comprehensive validation study has recently shown that both PBE0 and B3LYP hybrid functionals, when augmented by empirical dispersion contributions (*e.g.* D3), deliver remarkably accurate conformational energies for polypeptides.[33] MM calculations were carried out using the Gaussian09 program[31] and were based on the standard AMBER (ff99SB)[34,35] force field and on parameters specifically developed for cyclic α,α-dialkylated peptides, as detailed in a previous study.[29] All MD simulations were performed by using the SANDER module of the AMBER simulation package.[35] The AMBER force field and all our

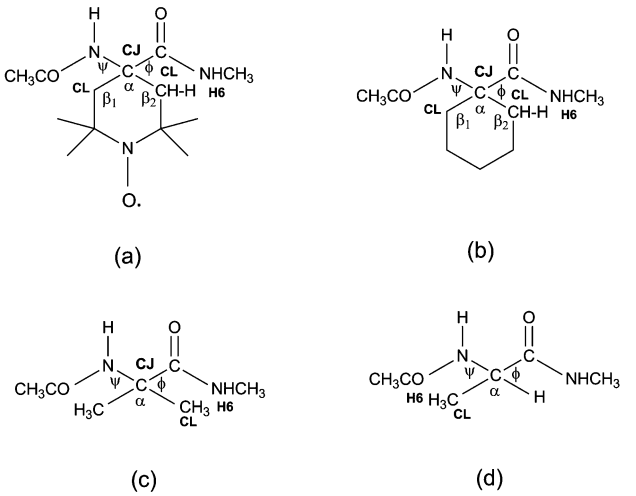

Fig. 1 Schematic illustration of the (a) TOAC, (b) Ac_6c (c) Aib and (d) Ala dipeptide analogues. New atom types introduced for modeling TOAC, Ac_6c and Aib based peptides are shown.

extensions are of maximally diagonal type and the total energy is given by eqn (1):

$$E_{\text{total}} = \sum_{\text{bonds}} K_r(r - r_0)^2 + \sum_{\text{angles}} K_\theta(\theta - \theta_0)^2 + \sum_{\text{dihedrals}} \frac{V_n}{2}[1 + \cos(n\phi - \gamma)] + \sum_{i<j}\left[\frac{A_{ij}}{R_{ij}^{12}} - \frac{B_{ij}}{R_{ij}^{6}} + \frac{q_i q_j}{\varepsilon_0 R_{ij}}\right] \quad (1)$$

where r_0 and θ_0 are the equilibrium bond length and bond angle; K_r, K_θ, and V_n are the force constants for the bond, bond angles and dihedral angles, respectively; n is multiplicity or periodicity, and γ is the phase angle for the torsional angle parameters. The nonbonded part of the potential is represented by a Lennard-Jones (6, 12) potential and interactions between partial atomic charges (q_i and q_j). ε_0 is the dielectric constant that takes into account the effect of the medium that is not explicitly represented. At the present stage of development, we rederived the van der Waals (vdW) and flexible torsion parameters only because test computations showed that these two factors contribute most significantly to the accuracy of the model for Aib. The vdW parameters of the CH_3 group are crucial for maintaining a reasonable balance between the possible secondary structures because errors could be cumulative in Aib containing protein models. Other parameters, including bond, angle and side-chain torsion parameters, are transferred from the existing AMBER ff99SB parameter set and our recent extension related to the cyclic α,α-dialkylated peptides.[29] The RESP atomic charges used for the Aib residue were determined at the PBE0/N07D level and were reported previously.[29]

Since the original AMBER ff99SB parameter set showed significant inconsistencies with respect to both QM and experimental studies of Aib peptides, we used here the same modified AMBER parameter set[34] related to the cyclic α,α-dialkylated peptides introduced by our group and described in ref. 29. The atom type, hereafter referred to as H6 (see Fig. 1), has been already introduced to describe hydrogen atoms attached to beta carbon atoms.[29] The H6 parameters essentially correspond to those listed in AMBER ff99SB for the HC atom type, with the exception of the van der Waals parameters, which have been re-optimized for the reasons sketched above.

Table 1 Optimized dihedral and van der Waals parameters

Dihedral angle	N of paths	$V_n/2$ (kcal mol^{-1})	γ (°)	n
CL–CJ–N–C	1	0.400	0.0	−3
CL–CJ–N–C	1	0.800	180.0	−2
CL–CJ–N–C	1	0.800	0.0	1

Lennard-Jones atom type	R (Å)	ε (kcal mol^{-1})
H6	1.280	0.0157

Note that $A_{ij} = \varepsilon_{ij}(R_{ij})^{12}$ and $B_{ij} = 2\varepsilon_{ij}(R_{ij})^6$; negative value of periodicity means that additional Fourier terms for the dihedral will follow, according to the standard nomenclature in the AMBER datafile.

In addition, we focused on the flexible torsion angle, CL–CJ–N–C (ψ). The purpose of the fitting was to ensure that the potential energy surface of Ac-Aib-NMe (calculated at the B3LYP-D3/N07T level) is adequately described. Dihedral energy parameters corresponding to backbone φ/ψ dihedrals (*i.e.*, V_n and γ) were treated as adjustable parameters. Once optimized, the flexible torsion parameters were kept fixed and used in a second round of fitting of the H6 vdW parameters. The final parameters describing torsion and vdW contributions are reported in Table 1. The overall RMSD with respect to the QM potential energy surface for the new parameters is 0.5 kcal mol^{-1} (see Table 2), well below the typical threshold of *ca.* 1.0 kcal mol^{-1}. Note that the original AMBER parameters provided a RMSD of 1.6 kcal mol^{-1}. The resulting parameters were tested both by comparison against QM data and by MD simulations of poly-Aib peptides in solvents with different polarity. Besides, MD simulations of a heptapeptide containing TOAC and Aib units have also been performed for the purpose of testing the modified force field to model the propensity to form different helical structures in water, as observed in EPR experiments. With the parameters presented here we recalculated the energies of the whole conformational ensemble of the TOAC and Ac_6c dipeptide analogues and obtained results very close to those previously reported[29] (Tables 6 and 7). Furthermore, test calculations on a few alanine (Ala) homopeptides have shown that the modification of vdW parameters of the CH_3 group (H6 and HL) does not affect, in this case, the relative stability of helix conformations ($3_{10\text{-R}}$, α_R and α_L) with respect to the original parameters (see Table 3).

2.2. Molecular dynamics simulations

Molecular dynamics simulations were carried out considering several peptides including Ac-$(Aib)_4$-NMe, Ac-$(Aib)_7$-NMe and double spin-labeled heptapeptide Fmoc-(Aib-Aib-TOAC)$_2$-Aib-OMe (Fmoc, fluorenyl-9-methoxycarbonyl; OMe, methoxy) (**1**) *in vacuo* and in aqueous solution, employing in the latter case the TIP3P model of water.[36] In the case of Ac-$(Aib)_4$-NMe, a simulation was also performed in chloroform using the AMBER parameters for chloroform. Note that the Ac-$(Aib)_4$-NMe peptide is one of the

Table 2 Comparison between energies and selected structural features of Ac-Aib-NMe as obtained from B3LYP-D3/N07T and MM calculations

	Energy			QM			MM		
No. chain[a]	QM	New-FF	Old-FF[b]	φ	ψ	CCJN	φ	ψ	CCJN
I γ	0.00	0.00	0.00	73	−56	112	70 (73)	−53 (−56)	113 (113)
II β	0.89	2.50	−0.03	180	180	106	180 (180)	180 (180)	109 (109)
III 3_{10}	2.53	2.29	−2.24	66	23	113	63 (56)	21 (9)	115 (116)
IV α	2.86	2.81	−0.15	61	38	111	64 (63)	40 (35)	112 (113)
V ε	3.84	4.66	4.24	−70	150	108	−70 (−70)	150 (150)	111 (111)
VI δ	4.81	4.54	0.16	−175	36	108	−177 (−176)	46 (25)	110 (110)
RMSD		0.48	1.63						

Energies are in kcal mol^{-1} and angles are in degrees. Main-chain torsion and valence angles are also given in the table for reference. Torsion and valence angles obtained by using the AMBER (ff99SB) force field are given in parentheses. [a] Peptide chain prediction. [b] Relative energies obtained by using the AMBER (ff99SB) force field.

Table 3 Comparison of relative energies (in kcal mol^{-1}) of the Ac-Ala-NMe and Ac-$(Ala)_9$-NMe obtained at AMBER and PBE/6-31G(d) levels of theory

No.	Chain	PBE0/6-31G(d)[a]	Old-FF[b]	FFvdW[c]
Ac-Ala-NME				
I	C7eq	0.00	0.00	0.00
II	C5	1.89	0.25	1.18
III	3_{10R}	6.09	2.41	2.89
IV	α_R	6.36	4.50	4.96
Ac-$(Ala)_9$-NMe				
I	α_R		0.00	0.00
II	3_{10R}		2.69	4.23
III	α_L		17.95	18.67

[a] QM data from ref. 14. [b] AMBER ff99SB. [c] AMBER ff99SB with vdW parameters of the CH_3 group refined for Aib.

smallest peptides that can potentially form two main-chain hydrogen bonds. These simulations were performed to examine the relative occurrence of peptide conformations in solution. Each system was equilibrated at 300 K and 1 bar in the canonical NVT ensemble starting from α or 3_{10} conformations. Solvent molecules were added in a periodic box of hexahedron shape (15 Å thickness). The minimum distances of the peptide atoms from box edges were set to 15 Å, leading to a total of 2081 water and 421 chloroform molecules. Preliminary short (500 steps) energy minimizations were carried out to avoid inappropriate atom–atom contacts. The initial velocities were assigned randomly according to a Gaussian distribution. The temperature was raised to 300 K from 50 K over 500 ps, and was maintained at 300 K using a Langevin algorithm with a collision frequency of 1.0 ps^{-1}. The equations of motion were integrated for 20 ns with a time step of 0.25 fs (*in vacuo*) and 1 fs (in water and chloroform). The subsequent analysis was based on equilibrated simulations, excluding an initial 500 ps equilibration phase. Particle Mesh Ewald[37,38] was used to account for the long-range electrostatic interactions, and the Lennard-Jones interactions were truncated at 10 Å. In the case of MD simulations *in vacuo* a cut-off of 20 Å was applied on long-range interactions. All bonds with hydrogen atoms were constrained using the SHAKE algorithm.[39]

2.3. PCM free energy calculations

Free energies of solvation in water and chloroform were computed by MM/PCM[40–44] calculations on 10 Aib polypeptides. Chloroform (in which Aib polypeptides are soluble) has been taken as a model low-polarity solvent. On the other hand, even if Aib oligopeptides are hardly soluble in water, the study of this solvent can give useful insights into the influence of an increase of the solvent polarity on the equilibrium between 3_{10}- and α-helices, since this effect should be significantly enhanced in water. According to PCM, the solvent is represented implicitly by a dielectric medium characterized by a relative dielectric constant of the bulk (4.90 for $CHCl_3$ and 78.39 for H_2O). A molecular-shaped surface contains the system under study (the solute) and separates it from the surrounding solvent. The PCM model calculates the free energy of solvation as the sum over three terms:

$$\Delta G_{solv} = \Delta G_{el} + \Delta G_{dr} + \Delta G_{cav}$$

These components represent the electrostatic (el) and the dispersion–repulsion (dr) contributions to the free energy, and the cavitation energy (cav). All three terms are calculated using a cavity defined through interlocking van der Waals-spheres centered at atomic positions. The cavity including the molecule, defined in terms of interlocking spheres centered on non-hydrogen atoms, is built by the GePol procedure[40] using the UAHF (United Atom for Hartree–Fock) atomic radii.[41] The cavitation term is determined using Pierotti's scaled particle theory,[42] while ΔG_{dr} is evaluated using semiempirical atom–atom parameters.[43] Finally, ΔG_{el} takes into account the solute–solvent electrostatic interaction.

3. Results and discussion

3.1. Assessment of the intrinsic conformational preferences of Aib homopolymers

The optimized Aib parameters to be used in conjunction with the standard AMBER ff99SB and our previous extension related to the cyclic α,α-dialkylated peptides are given in Table 1. The new parameters have been fitted to a QM derived potential energy surface of Aib dipeptide considered in different conformations. The local minima of the Aib dipeptide analogue as calculated at the B3LYP-D3/N07T level are given in Fig. 2. QM geometries were used as initial guess coordinates for MM calculations. The new parameters have been fitted to provide the smallest deviations in terms of geometries and relative energies. The energies and selected structural parameters for the optimized structures of Ac-Aib-NMe are presented in Table 2.

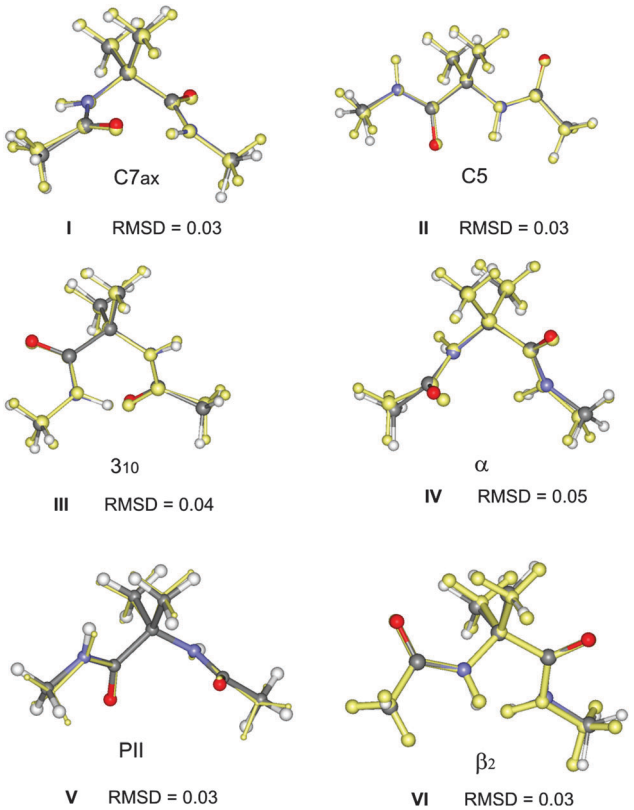

Fig. 2 Superpositions of the selected Ac-Aib-NMe geometries obtained from QM (yellow structure) and MM optimization. RMSD values are given in Å.

The new parameters produce conformers with an overall energy RMSD of 0.5 kcal mol^{-1} with respect to the QM reference calculations, while the original AMBER parameters provided a RMSD value of 1.6 kcal mol^{-1}. The maximum deviations between QM and MM main-chain torsion and valence angles are 10° and 3°, respectively (Table 2). Fig. 2 compares the molecular structures optimized at QM and MM levels. Inspection of Table 2 shows that the geometries and the stability trend predicted at the B3LYP-D3/N07T level compare well with the MM results, confirming the reliability of the new FF for the study of peptides with Aib residues. Helix conformers are less stable than β ($\varphi \approx 180°, \psi \approx 180°$) and γ ($\varphi \approx \pm 60°, \psi \approx \mp 60°$) conformers, the latter corresponding to the absolute energy minimum for Aib dipeptide; the β conformer is 2.5 kcal mol^{-1} less stable than the γ one. This is due to the fact that both β and γ conformers can form an intra-molecular hydrogen bond already at the dipeptide level. Note that the N–Cα–C angle is forced to a value few degrees smaller in the β conformer than the optimum value for a peptide residue (112°), in order to establish a hydrogen bond. This feature has also been observed in symmetrically disubstituted diethylglycine and di-*n*-propylglycine which adopt an extended β conformation in the solid state.[45,46] The 3_{10}-helix is relatively more stable (by 0.5 kcal mol^{-1}) than the α-helix with N–Cα–C valence angles about 3° larger than those in the α-helix, in agreement with theoretical and experimental data previously reported.[14,47,48] Finally, the least favored backbone conformations correspond to the ε ($\psi \approx \pm 60°, \psi \approx \mp 120°$) and δ ($\varphi \approx 180°, \psi \approx \pm 60°$) structures, which are 4.7 and 4.5 kcal mol^{-1}, respectively, less stable than the global energy minimum due to the lack of intra-molecular hydrogen bonding interactions. It can be seen from the results presented in Table 2 that the energy RMSD dropped from 1.6 to 0.5 kcal mol^{-1} after refitting the AMBER99SB parameters. At the same time, the energy difference between the γ and δ conformers became 4.5 kcal mol^{-1} after refitting, which is much closer to the QM result, 4.8 kcal mol^{-1}, than the standard AMBER99SB result (0.2 kcal mol^{-1}). Unlike standard AMBER99SB, the new force field reproduces very well the stability trend of different conformers in comparison to QM data.

Moreover, in order to test the transferability of the new Aib parameters, we have also computed conformational energies of increasingly longer Aib homopolypeptides and compared the results with available QM data.[14,18] Hence, MM calculations have been carried out on Ac-$(Aib)_n$-NMe, with n = 1–33. Since our main interest was to compare the helical forming propensity of the different homopolypeptides with QM data, in MM calculations the geometry of Aib residues was kept frozen to that optimized for the infinite homopolypeptide *in vacuo* by DFT calculations employing periodic boundary conditions (PBC):[14] accordingly, the backbone dihedral angles of 3_{10} and α helix conformations were fixed to ($\varphi, \psi = -51.3°, -25.3°$) and ($\varphi, \psi = -55.4°, -43.8°$), corresponding to right-handed 3_{10} and α-helices. Note, however, that because Aib is achiral, both left- and right-handed helices of homopolypeptides are energetically equivalent. Table 4 shows that the 3_{10} helix is favored with respect to α-helix for all values of n. These results suggest that the extra hydrogen bond makes the 3_{10}-helix conformations the most stable *in vacuo*, in good agreement with previous QM studies which also predicted the 3_{10} helix to be more stable than the α-helix by about 0.5 kcal mol^{-1} per residue.[14] From Table 4, it is apparent that the advantage of using the refitted Fourier coefficients and vdW parameters is even more pronounced, with an energy RMSD reduced from 7.5 to 0.4 kcal mol^{-1}, which is within the usual accuracy required for reliable predictions of large molecular systems. These results are fully consistent with previous experiments where it has

Table 4 Energies (in kcal mol^{-1}) obtained at MM and PBE0/6-31G(d)[a] levels of theory for the α-helix relative to the 3_{10}-helix of homopolypeptides of Ac-$(Aib)_n$-NMe

	PBE0/6-31G(d)	New-FF	Old-FF[b]
Chain	Gas phase		
$(Aib)_1$	0.51	0.50	1.90
$(Aib)_2$	2.85	1.96	5.61
$(Aib)_3$	3.48	3.82	9.48
$(Aib)_4$	5.28	4.96	11.78
$(Aib)_5$	6.23	5.61	15.89
$(Aib)_6$	6.81	6.22	18.83
$(Aib)_7$	7.17	6.82	20.23
$(Aib)_8$	7.41	7.10	25.78
$(Aib)_{10}$		7.55	30.92
$(Aib)_{33}$		12.92	68.30
RMSD		0.36	7.45

[a] QM data from ref. 18. [b] AMBER (ff99SB) force field.

Table 5 Solvation free energies (in kcal mol^{-1}) obtained at AMBER and PBE0/6-31G(d)[a] levels of theory for the α-helix relative to the 3_{10}-helix of homopolypeptides of Ac-$(Aib)_n$-NMe

	PBE0/6-31G(d)	New-FF	PBE0/6-31G(d)	New-FF
Chain	PCM/WATER		PCM/$CHCl_3$	
$(Aib)_1$	−0.75	−1.10	−0.59	−0.68
$(Aib)_2$	−2.76	−2.77	−1.38	−2.50
$(Aib)_3$	−3.26	−5.32	−2.54	−2.90
$(Aib)_4$	−6.54	−8.10	−4.86	−5.80
$(Aib)_5$	−10.17	−11.65	−7.31	−7.84
$(Aib)_6$	−12.79	−14.67	−9.34	−9.27
$(Aib)_7$	−15.06	−17.01	−10.64	−10.88
$(Aib)_8$	−17.05	−18.81	−12.05	−11.84
RMSD		1.18		0.52

[a] QM data from ref. 18.

been shown that the 3_{10}-helix should be the most favorable for poly-Aib in low polarity solvents.[15–17]

AMBER/PCM calculations in water and $CHCl_3$ are shown in Table 5. Solvent effects now lead to a preference for the α-helix over the 3_{10}-helix in both cases, with a similar dependence on the peptide length. A detailed comparison of the AMBER/PCM and PBE0/PCM results indicates that the new FF provides quite accurate solvation energies in $CHCl_3$ and slightly underestimates the electrostatic contribution with respect to PBE0/6-31G(d)/PCM in aqueous solution. The RMSD values with respect to QM data are 1.2 and 0.5 kcal mol^{-1} for water and $CHCl_3$, respectively, which supports the suitability of the new force field to describe solvation free energies in large molecular systems.

Table 6 Comparison between energies and selected structural features of the Ac-Ac_6c-NMe obtained at PBE0/N07D and AMBER levels of theory

	Energy				QM			MM			
No. chain[a]	QM	New-FF	Old-FF	AMBER ff99SB	φ	ψ	CLCJN	φ	ψ	CLCJN	Ring[b]
I γ	0.00	0.00	0.00	0.00	−73	54	112	−71 (−71)	60 (61)	112 (113)	$^4C_1$
II γ	0.25	0.02	0.02	0.50	−73	69	109	−70 (−71)	68 (69)	111 (111)	$^1C_4$
III 3_{10}	2.51	3.96	3.95	0.15	−72	−16	113	−71 (−58)	−16 (−16)	114 (114)	$^4C_1$
IV ε	2.92	2.95	4.23	1.25	−57	128	107	−57 (−57)	127 (127)	110 (110)	$^4C_1$
V β	3.45	0.82	1.55	−4.48	180	180	103	170 (180)	170 (180)	105 (106)	$^1C_4$
VI α	4.00	4.92	5.15	1.16	−63	−34	110	−62 (−64)	−35 (−34)	112 (112)	$^1C_4$
VII γ	5.27	5.91	5.46	7.22	−71	58	111	−68 (−70)	60 (61)	113 (112)	$^6T_2$
VIII γ	5.71	5.55	4.85	7.21	−75	51	111	−71 (−72)	60 (60)	112 (112)	$^2T_6$
IX γ	5.76	7.22	6.40	7.94	−74	52	111	−70 (−71)	62 (62)	111 (111)	$^3T_1$
X δ	5.85	5.43	8.59	3.26	−178	52	106	−176 (−178)	60 (60)	108 (109)	$^1C_4$
XI β	6.55	4.30	6.05	−1.20	180	−180	102	170 (−179)	−170 (−180)	105 (105)	$^4C_1$
XII 3_{10}	7.83	9.66	8.95	7.27	−66	−26	112	−62 (−64)	−19 (−20)	114 (114)	$^6T_2$
XIII β	8.32	5.84	7.41	−1.00	−169	164	103	−160 (−164)	156 (166)	105 (106)	$^2T_6$
XIV 3_{10}	8.41	8.41	8.91	6.46	−71	−22	112	−64 (−66)	−22 (−22)	114 (114)	$^2T_6$
XV ε	9.15	9.05	9.05	7.90	−58	136	107	−58 (−58)	136 (136)	110 (110)	$^3T_1$
RMSD		1.28	1.16	4.01							

Energies are in kcal mol^{-1} and angles are in degrees. Main-chain torsion and valence angles are also given in the table for reference. Torsion and valence angles obtained by using the old force field[29] are given in parentheses. [a] Peptide chain predictions. [b] Cremer–Pople notation.[50]

Table 7 Comparison between energies and selected structural features of the Ac-TOAC-NMe obtained at PBE0/N07D and AMBER levels of theory

	Energy			QM			MM			
No. chain[a]	QM	New-FF	Old-FF	φ	ψ	CLCJN	φ	ψ	CLCJN	Ring[b]
I γ	0.00	0.00	0.00	−73	58	110	−70 (−71)	64 (64)	110 (111)	$^1C_4$
II γ	0.83	0.87	0.20	−75	58	110	−72 (−73)	64 (64)	111 (111)	$^2T_6$
III γ	0.83	1.20	0.27	−73	67	109	−68 (−71)	64 (66)	111 (111)	$^6T_2$
IV γ	1.19	0.38	1.01	−75	71	107	−71 (−74)	76 (79)	109 (107)	$^4C_1$
V γ	1.81	2.16	1.87	−72	57	111	−70 (−71)	57 (57)	112 (112)	$^{1,4}B \Leftrightarrow {}^4E$[c]
VI β	2.39	0.68	3.58	−180	155	103	−178 (−177)	156 (156)	105 (106)	$^2T_4$
VII ε	2.60	2.76	2.85	−61	120	106	−61 (−61)	120 (120)	109 (109)	$^1C_4$
VIII 3_{10}	2.60	4.86	4.86	−72	−16	112	−67 (−67)	−17 (−17)	114 (114)	$^1C_4$
IX 3_{10}	3.71	5.38	5.42	−64	−27	112	−62 (−62)	−27 (−27)	115 (114)	$^{1,4}B \Leftrightarrow {}^4E$
X α	3.88	6.43	5.55	−63	−34	109	−65 (−65)	−27 (−27)	113 (113)	$^6T_2$
XI α	4.07	6.17	5.91	−66	−31	110	−65 (−66)	−31 (−31)	113 (113)	$^2T_6$
XII ε	5.18	3.54	3.57	−60	138	109	−60 (−60)	138 (138)	109 (109)	$^2T_6$
XIII α	5.72	7.95	7.88	−58	−44	108	−63 (−66)	−51 (−54)	111 (111)	$^4C_1$
XIV δ	6.76	5.72	8.33	−180	−66	103	177 (177)	−73 (−73)	105 (106)	$^4C_1$
XV β	7.19	6.24	7.06	−150	157	102	−149 (−149)	153 (157)	103 (105)	$^2T_6$
RMSD		1.46	1.32							

Energies are in kcal mol^{-1} and angles are in degrees. Main-chain torsion and valence angles are also given in the table for reference. [a] Peptide chain prediction; torsion and valence angles obtained by using the old force field[29] are given in parentheses. [b] Cremer–Pople convention.[50] [c] Between $^{1,4}B$ and ^4E.

3.2. Validation of the new parameters on cyclic α,α-dialkylated dipeptides

Here, we want to show that the new modifications of the FF do not affect significantly the energetics and geometries of the same cyclic systems considered in our previous study, namely Ac-Ac$_6$c-NMe and Ac-TOAC-NMe.[29] The energies and selected structural parameters for the reoptimized structures of Ac-Ac$_6$c-NMe and Ac-TOAC-NMe are presented in Tables 6 and 7, respectively, where results obtained from the new and old force field[29] and, for comparison, the standard AMBER ff99SB are reported. Reference QM data are also reported, as obtained from ref. 29. The RMSD between the QM and MM energies of Ac$_6$c and TOAC dipeptide analogues, as obtained from 15 different conformers using the new parameters, are 1.3 and 1.5 kcal mol^{-1}, respectively. Similarly, small deviations have been obtained by using the previous force field reported in ref. 29 (see Tables 6 and 7), whereas a significant improvement over standard AMBER is observed. The differences in main-chain torsion and valence angles between the QM and MM optimized structures refined with the new force-field are less than 10° and 3° for both Ac$_6$c and TOAC dipeptides.

3.3. Molecular dynamics simulations of Aib homopolypeptides

The refined parameters were also tested by MD simulations of Ac-(Aib)$_4$-NMe and Ac-(Aib)$_7$-NMe homopolypeptides *in vacuo* and water. Furthermore, a simulation of the tetrapeptide in chloroform was also performed. The 3_{10}- and α-helix structures of Ac-(Aib)$_4$-NMe optimized by MM computations are shown in Fig. 3. The right-handed 3_{10}-helical conformation of the molecule is stabilized by three intra-molecular 3,1 H-bonds, while the α-helical conformation of the molecule is stabilized by two intra-molecular 4,1 H-bonds. Fig. 4–6 show the normalized φ–ψ angle distributions of the tetrapeptide along a MD trajectory at 300 K in the gas phase and in solution. A striking feature of the MD trajectories *in vacuo* is the presence of several transitions for each residue of the tetrapeptide. The most populated regions of the Ramachandran map (Fig. 7) of each residue are 3_{10}/α (±60°, ±30°)/(±60°, ±40°) and γ (±70°, ∓70°). The φ1 torsion was more flexible because Aib1 was at the C-terminus. During the 20 ns simulations, Aib1 and Aib2 residues underwent transitions between left-handed and right-handed helical regions. The φ and ψ torsions of Aib were mostly centered at the ±60° and ±40° regions, but Aib1 also explored regions around 180°. The result is consistent with experimental X-ray

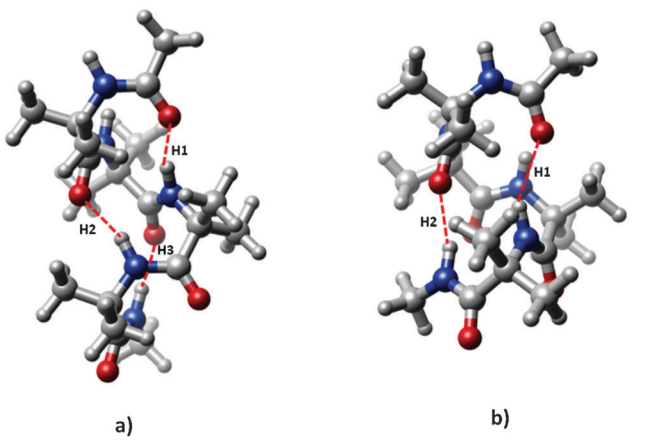

Fig. 3 Optimized (a) 3_{10}-helix and (b) α-helix structures of Ac-(Aib)$_4$-NMe as obtained from MM optimization.

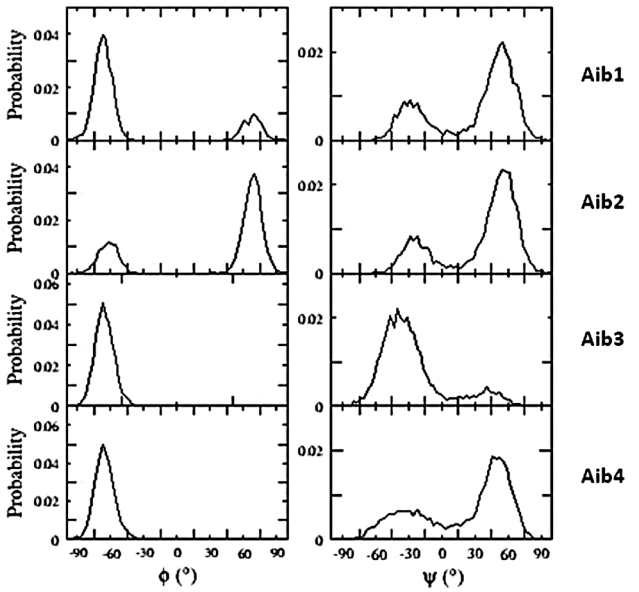

Fig. 4 Normalized φ–ψ angle distributions of Ac-(Aib)$_4$-NMe *in vacuo* during 20 ns MD simulations. Standard deviations for φ are in the range σ = 5–10°. Standard deviations for ψ are in the range σ = 5–10°.

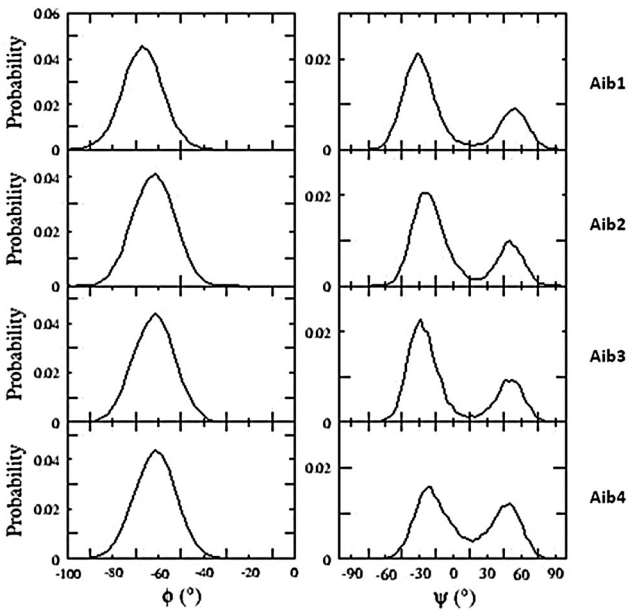

Fig. 5 Normalized φ–ψ angle distributions of Ac-(Aib)$_4$-NMe in chloroform during 20 ns MD simulations. Standard deviations for φ are in the range σ = 5–10°. Standard deviations for ψ are in the range σ = 5–10°.

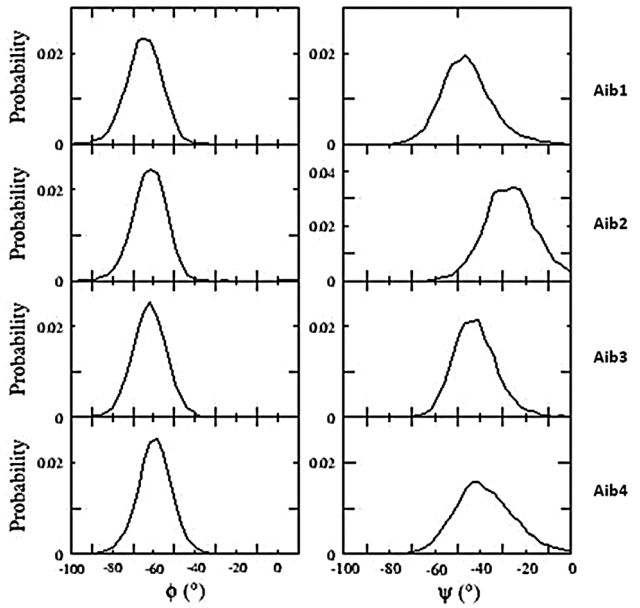

Fig. 6 Normalized φ–ψ angle distributions of Ac-(Aib)$_4$-NMe in water during 20 ns MD simulations. Standard deviations for φ are in the range σ = 5–10°. Standard deviations for ψ are in the range σ = 5–10°.

data of Aib tetrapeptide where the helicity of the terminal Aib residue is inverted with positive values of φ and ψ.[48] A similar conformational behavior was observed in chloroform where the most favorable structures of all residues correspond to α-helix (±60°, ±30°) and γ (±70°, ∓70°) regions (see Fig. 7). As expected, the ψ angle distribution undergoes the most relevant change by shifting to lower values in going from a nonpolar to a polar solvent. As seen in Fig. 6 and 7, the allowed conformational states of Ac-(Aib)$_4$-NMe in water are predicted in the regions of the helices (centered at (φ, ψ) = (±60°, ±40°)). The stability of the α and 3$_{10}$ conformations found in the 20 ns MD simulations has been confirmed by the presence of H-bonds (see Table 8). We only monitored the occurrence of major H-bonds (with a presence larger than 30%) in the 20 ns simulations.

The 3$_{10}$- and α-helix structures of Ac-(Aib)$_7$-NMe optimized by MM computations are shown in Fig. 8. Fig. 9 and 10 (bottom) show the MD results for heptapeptide *in vacuo* and in aqueous solution. The main geometric parameters describing the H-bond pattern in helixes are also reported in Table 9. In agreement with previous experimental and computational determinations, *in vacuo* conformational sampling obtained from a 20 ns MD is mainly restricted to the 3$_{10}$ region (centered at (φ, ψ) = (±60°, ±30°)). This result is in agreement with the well-known propensity of the Aib homopolypeptides to adopt 3$_{10}$ conformation in a nonpolar environment, irrespective of the number of residues. The preference of Aib homopolymers for 3$_{10}$-helix over α-helix is mainly due to the severe distortion of the α-helix induced by methyl–methyl interresidue repulsions. Confirming the trend found at the DFT/

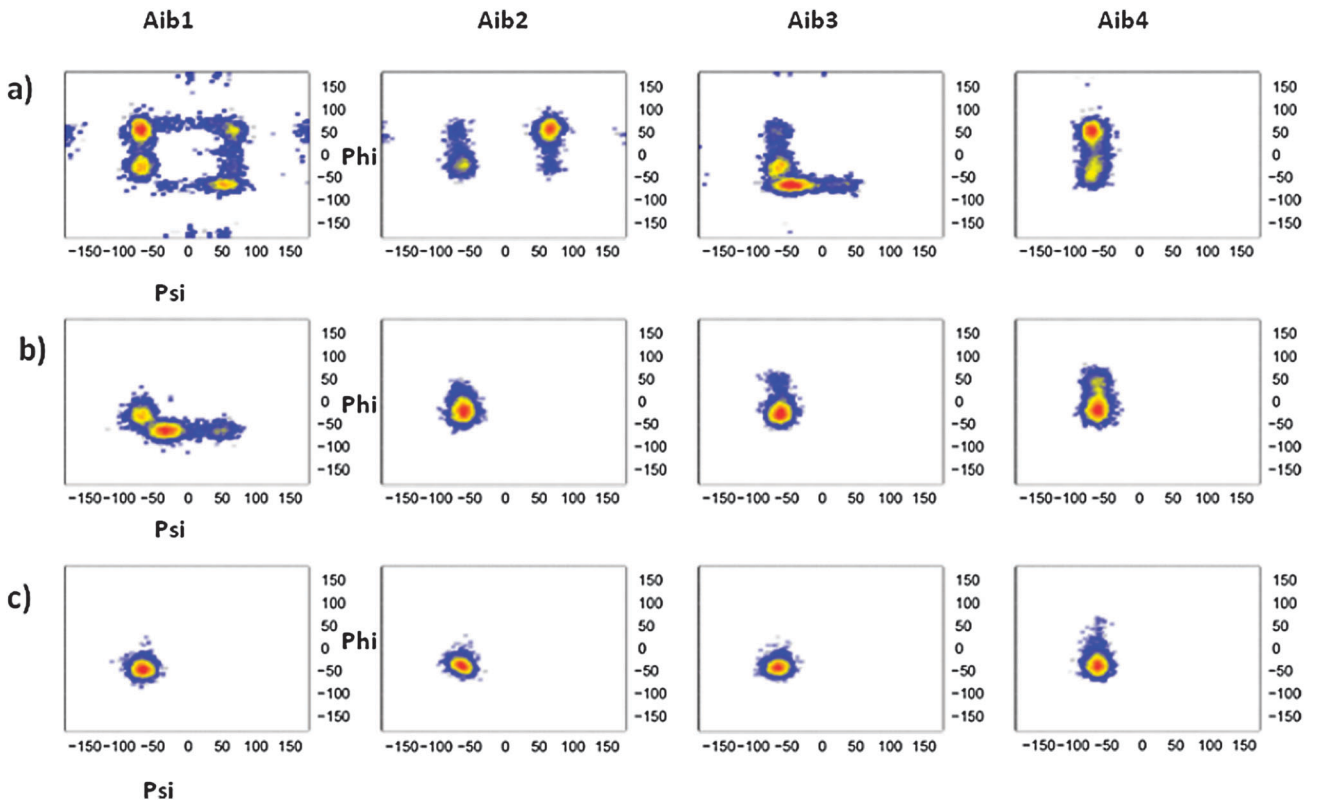

Fig. 7 Ramachandran maps of the Ac-(Aib)$_4$-NMe obtained from MD trajectories *in vacuo* (a), (b) in chloroform and (c) in water. Red indicates the highest percentage of population, and white indicates that a region was not populated.

Table 8 Computed intramolecular H-bonds (in Å) as obtained from MD simulations (averages) of Ac-(Aib)$_4$-NMe

Helix		H1	H2	H3
3_{10}	MD (gas)	2.20 (0.4)	2.25 (0.2)	2.29 (0.2)
3_{10}	MD ($CHCl_3$)	2.29 (0.3)	2.24 (0.3)	2.47 (0.6)
3_{10}	MD (H_2O)	2.72 (0.5)	2.70 (0.4)	2.69 (0.4)
α	MD (H_2O)	2.39 (0.4)	2.39 (0.4)	

Standard deviations are given in parentheses.

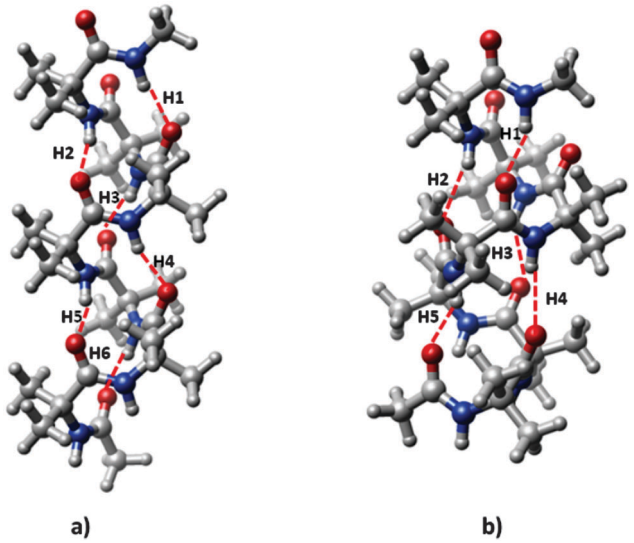

Fig. 8 3_{10}-Helix (a) and α-helix (b) structures of Ac-(Aib)$_7$-NMe, optimized by MM computations.

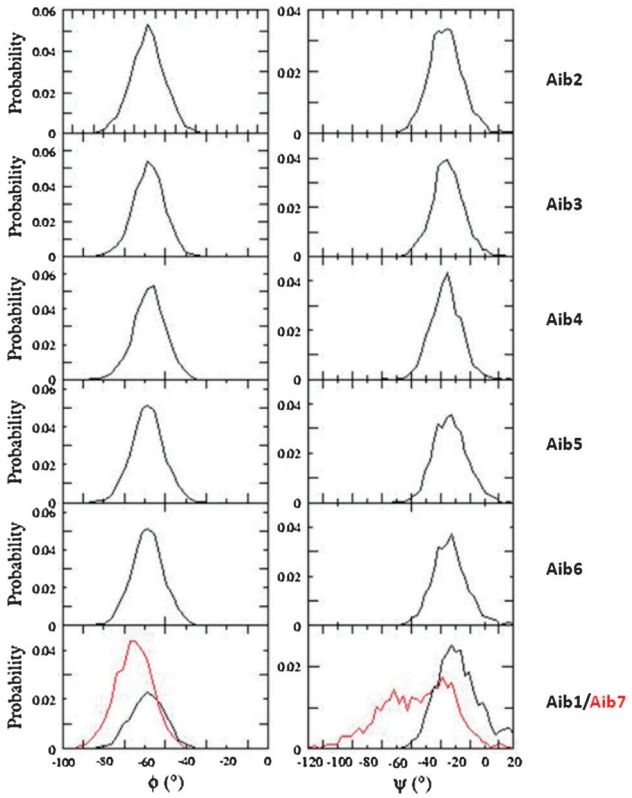

Fig. 9 Normalized φ–ψ angle distributions of Ac-(Aib)$_7$-NMe *in vacuo* during 20 ns MD simulations. Standard deviations for ψ are in the range σ = 5–10°.

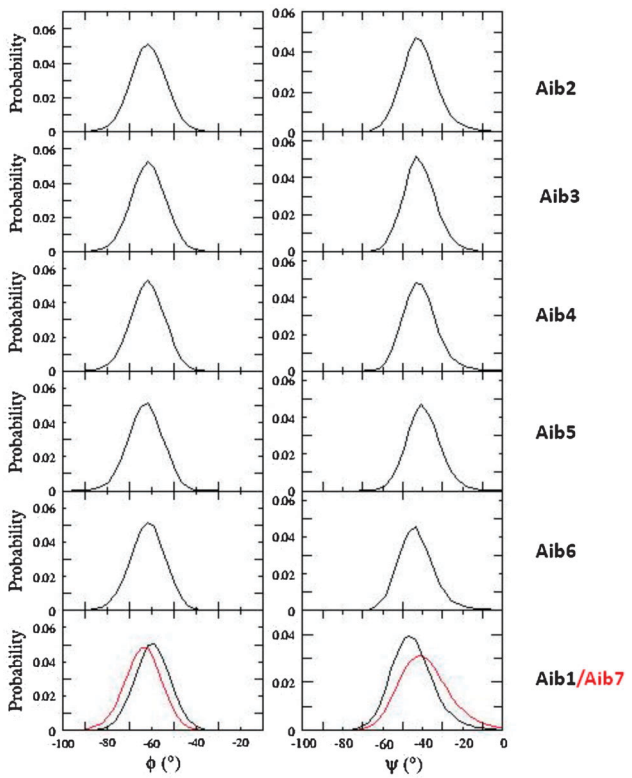

Fig. 10 Normalized φ–ψ angle distributions of Ac-(Aib)$_7$-NMe in water during 20 ns MD simulations. Standard deviations for ψ are in the range σ = 5–10°.

PCM level, the α-helix is favored in aqueous solution. Analysis of the structures from simulations revealed little formation of *i*, *i* + 3 3_{10} hydrogen bonds (around 30%). As already evidenced, in the α-helix polar groups (mainly oxygen atoms) are better exposed to the solvent. This behavior is consistent with previous studies[19–21] showing that, in peptides where the α/3_{10}-helix equilibrium exists, solvents with high polarity usually favor the α-helix formation, while the 3_{10}-helix is often found in low polarity solvents.

3.3.1. 3_{10}/α helix transitions. The solvation free energy profile for interconverting the 3_{10}- and α-helix form of Aib heptapeptide in aqueous solution, as obtained from MM/PCM calculations, is shown in Fig. 11. The convergence of the calculated free energies was ascertained by scanning the free energy curve over configurations found by restraining the φ and ψ angles of the peptide structure, where φ and ψ were rotated every 1° to cover the complete 3_{10} and α helix periods of both backbone dihedrals. Advantage has been taken of the similar φ values for α- and 3_{10}-helices to permit convenient use of ψ as the reaction coordinate. Note that both the α and 3_{10} forms were found to be local minima of the free energy surface, with the α conformation showing a lower energy in solution by 16.2 kcal mol^{-1}. The computed small barrier, about 1.6 kcal mol^{-1}, for the transition from 3_{10}- towards α-helix is consistent with

Table 9 Computed intramolecular H-bonds (in Å) as obtained from MD simulations (averages) of Ac-$(Aib)_7$-NMe

Helix		H1	H2	H3	H4	H5	H6
3_{10}	MD (gas)	2.2 (0.4)	2.25 (0.2)	2.29 (0.2)	2.28 (0.3)	2.23 (0.3)	2.40 (0.5)
3_{10}	MD (H_2O)	2.83 (0.5)	2.81 (0.5)	2.73 (0.3)	2.75 (0.4)	2.25 (0.2)	2.8 (0.4)
α	MD (H_2O)	2.37 (0.4)	2.50 (0.4)	2.55 (0.3)	2.49 (0.3)	2.33 (0.4)	

Standard deviations are given in parentheses.

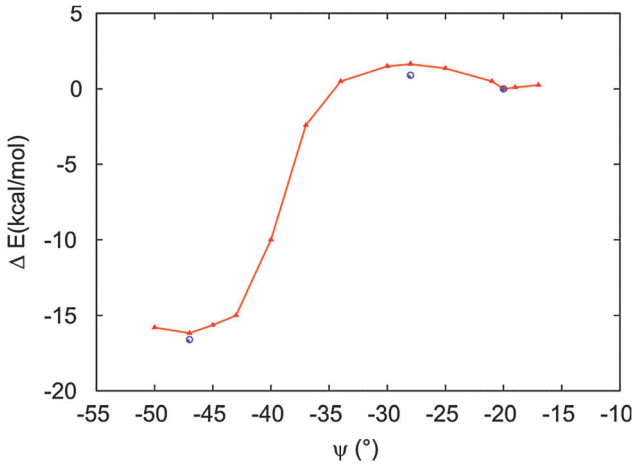

Fig. 11 Free energy profile obtained from MM/PCM simulations in aqueous solution for the 3_{10}- to α-helix interconversion of Aib heptapeptide. The exact values of the minima are α = (−54°, −47°) and 3_{10} = (−51°, −20°). The blue dots correspond to QM/PCM values.

the behavior observed in the MD calculations. In addition, relative free energies computed at the PBE0/N07D/PCM level in aqueous solution for selected optimized structures are also presented in Fig. 11 for comparison. Differences between QM and MM values are smaller than 1 kcal mol^{-1}, in particular the energy difference between corresponding 3_{10} structure and the transition state is 0.9 kcal mol^{-1} at the QM level, in fair agreement with the MM value of 1.6 kcal mol^{-1}. Such a result further confirms the transferability of the developed force field not only toward longer polypeptide chains with respect to the dipeptide analogue adopted in the fitting procedure (see Section 2) but also for modeling intermediate structures out of local energy minima, therefore opening the route towards a more detailed investigation of poly-Aib structural transitions occurring in solution.

3.4. Double spin-labeled heptapeptide Fmoc-(Aib-Aib-TOAC)$_2$-Aib-OMe: comparison of MD simulations with EPR data

One of the goals of the new Aib force field parameterization was to improve the agreement with experimental (EPR) and QM data for the double spin-labeled, terminally protected heptapeptide Fmoc-(Aib-Aib-TOAC)$_2$-Aib-OMe (**1**) in different solvents.[29,49] QM geometry optimizations have shown, in agreement with EPR data, that the preferential conformation of **1** changes from 3_{10} to α-helix when the polarity and the hydrogen bonding capability of the solvent do increase: the α-helix predominates in protic solvents and at low temperature, whereas the 3_{10}-helix is favored in aprotic solvents. The X-ray crystal structure of **1** has been solved and corresponds to the 3_{10} helix structure.[49] MD simulations of such a heptapeptide were performed *in vacuo* and in water starting from a 3_{10} helix structure. As observed before,[29] the 3_{10} helix is the most favored structure in the gas phase (Fig. 12), with all the geometrical parameters averaged over the MD trajectories in good agreement with those derived from X-ray analysis and QM computations, including the hydrogen bonding network (see Table 10). On the other hand, two different energy minima were obtained in aqueous solution, corresponding to 3_{10}- and α-helical arrangements of the peptide backbone (Fig. 13 and 14). The simulations show a significantly larger (around 80%) population of α-helix with respect to 3_{10} helix and hence provide a good quantitative agreement with experimental EPR results.[49]

The average geometries of 3_{10}- and α-helix obtained from MD simulations of **1** are in good agreement with those predicted by QM geometry optimizations[49] (see Table 10): the differences in the non-bonded distances of atoms, including NO moieties, are never larger than 0.5 Å. The main geometric parameters describing the H-bonding pattern in both helixes are also reported in Table 10. Normalized φ–ψ angle distributions obtained from the aqueous solution simulations are also presented in Fig. 14. Again, there is good agreement between the calculated backbone dihedrals and the corresponding QM data.[49] The results obtained in water consistently show that the new extended force field represents a remarkable improvement with respect to its original version and provides a description of structural and dynamical properties of the doubly labeled heptapeptide in good agreement with available experiments.

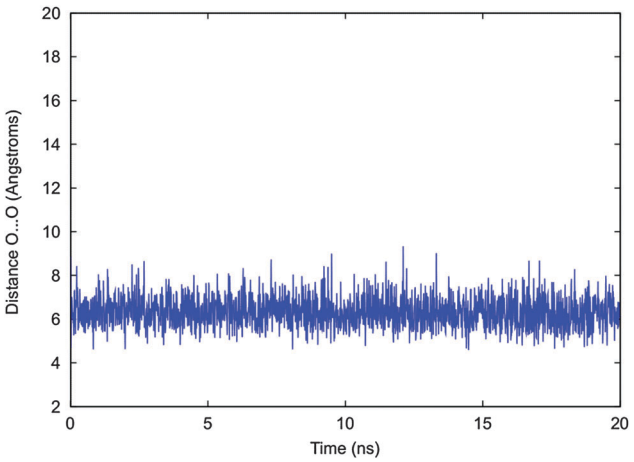

Fig. 12 Conformational behavior of heptapeptide **1** during the 20 ns MD simulation performed *in vacuo*: O···O distance as a function of simulation time.

Table 10 Comparison between computed geometrical parameters (in Å) of **1** as obtained from MD simulations (averages) and QM calculations or experimental data taken from ref. 49

Helix		N1···N2[a]	O1···O2[b]	H1	H2	H3	H4	H5
3_{10}	MD (gas)	6.13 (0.4)	6.35 (0.6)	1.92 (0.2)	2.22 (0.2)	2.26 (0.2)	1.98 (0.2)	2.22 (0.2)
3_{10}	MD (H_2O)	6.21 (0.4)	6.48 (0.6)	2.01 (0.3)	2.51 (0.4)	2.50 (0.3)	2.03 (0.2)	2.50 (0.4)
α	MD (H_2O)	7.91 (0.2)	9.35 (0.3)	1.95 (0.2)	2.40 (0.3)	2.10 (0.3)	2.14 (0.2)	—
3_{10}	[1]QM (gas)	6.57	6.80	2.02	2.11	2.05	2.12	2.06
3_{10}	[1]QM (H_2O)	6.51	6.74	1.96	2.02	2.02	2.04	1.99
α	[1]QM (H_2O)	7.97	9.27	1.97	2.13	2.18	2.19	—
3_{10}	[1]X-ray	6.40	6.59	2.22	2.14	2.22	2.18	2.17

[1] Values from ref. 49. Standard deviations are given in parentheses. [a] N1 and N2 are nitrogen atoms of NO moieties of TOAC residues at positions $i + 3$ and $i + 6$ of heptapeptide **1**, respectively. [b] O1 and O2 are oxygen atoms of NO moieties of TOAC residues at positions $i + 3$ and $i + 6$ of heptapeptide **1**, respectively.

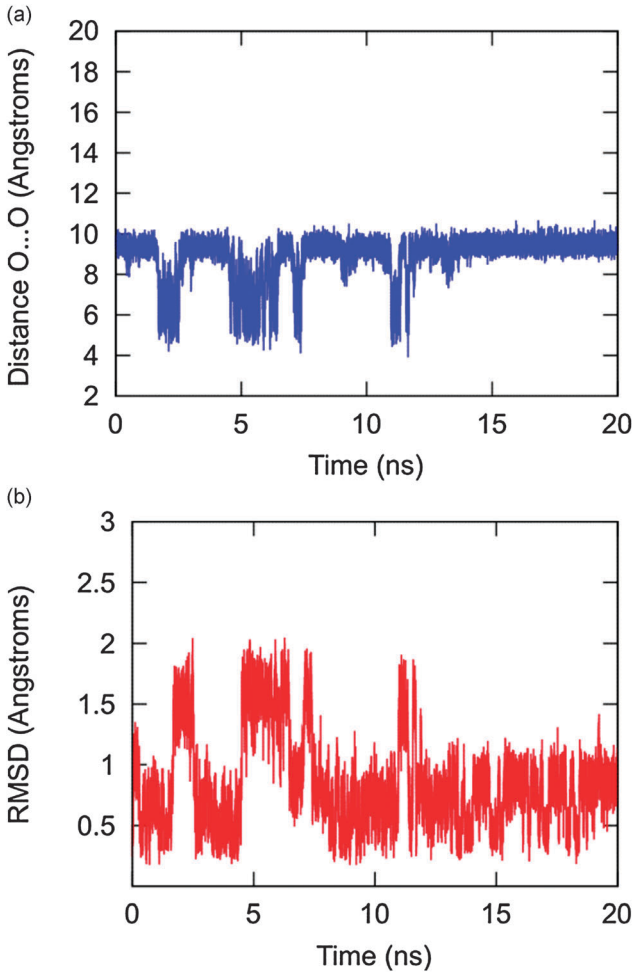

Fig. 13 Conformational behavior of **1** during the 20 ns MD simulation performed in water: (a) O···O distance as a function of simulation time; (b) RMSD of the backbone atoms with respect to the α-helix structure of the same heptapeptide.

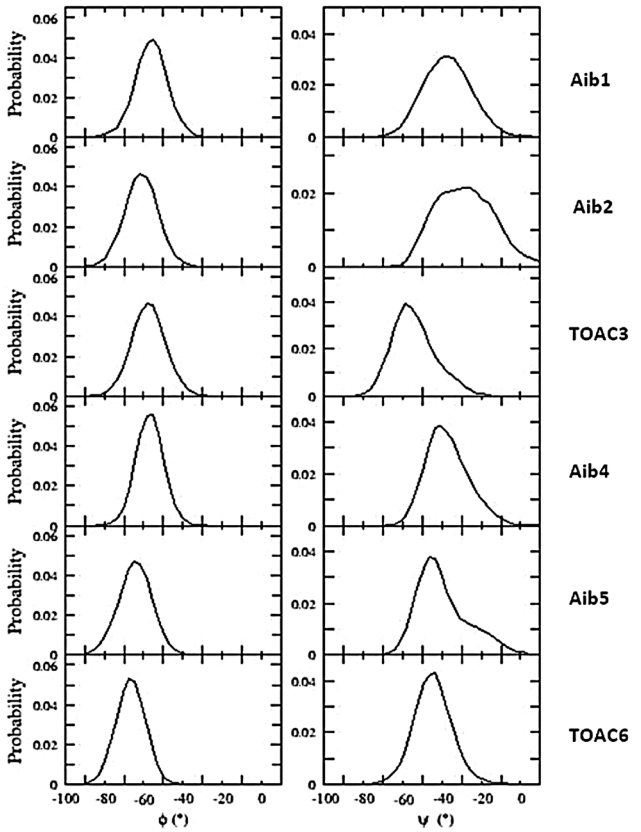

Fig. 14 Normalized φ–ψ angle distributions of **1** in water. Standard deviations for φ are in the range σ = 5–10°. Standard deviations for ψ are in the range σ = 5–9°.

4. Conclusions

We have derived and validated enhanced parameters for the AMBER force field to be used for α,α-dialkylated residues with cyclic and linear side chains. The α-aminoisobutyric residue appears to be problematic for the original AMBER parametrization possibly due to a poor description of the intra-molecular interactions involving methyl groups. A reduced number of parameters was optimized with reference to new DFT data including an empirical dispersion correction and was validated for several dipeptide analogues and polypeptides using both QM and experimental reference data, when available. The corrections introduced here for Aib range between 1 and 21 kcal mol^{-1}, among the considered peptides, and can thus have a significant impact on the stability of proteins. On the other hand, the results for α,α-dialkylated cyclic and alanine dipeptide analogues are very close to those delivered by our previous reparametrization and by standard AMBER,

respectively. Coming to longer polypeptides, our results confirm previous conclusions based on QM computations in suggesting that, *in vacuo*, poly-Aib adopts a 3_{10} right- or left-handed helical conformation, with the 3_{10}-helix always slightly more stable than the α-helix.[14] Solvent effects on the conformational preferences of Aib homopolymers have been investigated coupling the polarizable continuum model (PCM) with the MM representation of solute. MM/PCM calculations predict, in agreement with previous PBE0/6-31G(d)/PCM calculations,[18] that the α-helix becomes the preferred structural motif in aqueous solution. This is also supported by MD simulations of oligomers with 4 and 7 Aib residues, where both α and 3_{10} structures have been observed, but with a significantly higher populations of the α-helix. The performances of the new force field were further demonstrated by accurately reproducing the stable secondary structures of the terminally blocked double spin-labeled heptapeptide Fmoc-(Aib-Aib-TOAC)$_2$-Aib-OMe *in vacuo* and in aqueous solutions. The excellent agreement between MD and spectroscopically derived results provides a firm base for further applications of the refined force field parameter set for investigation of the macromolecular structure of spin labeled systems and conformational flexibility through electron paramagnetic resonance methods.

Because the new parameters represent a remarkable improvement and did not reveal any artifactual behavior in the several tests performed, we recommend the use of the new AMBER-GBB force field (see also ref. 29) to study any protein containing α,α-dialkylated residues with cyclic and/or linear side chains. Parameters can be freely downloaded from the http://dreams.sns.it website.

Acknowledgements

G.B. acknowledges the financial support of the INFN and the Italian Ministry for Education, University and Research (MIUR) through the FIRB Futuro in Ricerca ''SUPRACARBON'' (contract no. RBFR10DAK6). V.B. acknowledges the European Research Council (ERC) for financial support through the Advanced Grant DREAMS: 320951 ''Development of a Research Environment for Advanced Modelling of Soft matter''. S.G. acknowledges support of Italian MIUR and the Serbian Ministry of Education and Science (Grant No. 172035). The COST Action CM1002: ''COnvergent Distributed Environment for Computational Spectroscopy (CODECS)'' is also acknowledged by all the authors.

References

1 G. Jung, W. A. Konig, D. Leibfritz, T. Ooka, K. Janko and G. Boheim, *Biochim. Biophys. Acta*, 1976, **433**, 164–171.
2 W. A. Konig and M. Aydin, in *Peptides 1980*, ed. K. Brunfeld, Scriptor, Copenhagen, 1981, pp. 711–718.
3 P. Balaram, *Curr. Opin. Struct. Biol.*, 1992, **2**, 845–851.
4 B. Koksch, N. Sewald, K. Burger and H. D. Jakubke, *Biomed. Life Sci.*, 1996, **11**, 425–434.
5 C. Toniolo, M. Crisma, F. Formaggio and C. Peggion, *Biopolymers*, 2001, **60**, 369–419.
6 R. O. Fox Jr and F. M. Richards, *Nature*, 1982, **300**, 325–330.
7 E. Benedetti, B. Di Blasio, V. Pavone, C. Pedone, A. Bavoso, C. Toniolo, G. M. Bonora, M. T. Leplawy and P. M. Hardy, *Proc. Int. Symp. Biomol. Struct. Interact., Suppl. J. Biosci.*, 1985, **8**, 253–262.
8 B. V. Prasad and P. Balaram, *Crit. Rev. Biochem.*, 1984, **16**, 307–348.
9 I. L. Karle and P. Balaram, *Biochemistry*, 1990, **29**, 6747–6756.
10 B. Di Blasio, V. Pavone, M. Saviano, A. Lombardi, F. Nastri, C. Pedone, E. Benedetti, M. Crisma, M. Anzolin and C. Toniolio, *J. Am. Chem. Soc.*, 1992, **114**, 6273–6278.
11 T. S. Yokum, T. J. Gauthier, R. P. Hammer and M. L. McLaughlin, *J. Am. Chem. Soc.*, 1997, **119**, 1167–1168.
12 V. Barone, F. Lelj, A. Bavoso, B. Diblasio, P. Grimaldi, V. Pavone and C. Pedone, *Biopolymers*, 1985, **24**, 1759–1767.
13 A. Bavoso, E. Benedetti, B. Di Blasio, V. Pavone, C. Pedone, C. Toniolo and G. M. Bonora, *Biochemistry*, 1986, **83**, 1988–1992.
14 R. Improta, V. Barone, K. N. Kudin and G. E. Scuseria, *J. Am. Chem. Soc.*, 2001, **123**, 3311–3322.
15 B. R. Malcom, *Biopolymers*, 1977, **16**, 2591.
16 B. R. Malcom, *Biopolymers*, 1982, **22**, 319.
17 S. Krimm, A. M. Owivedi, Proc. I.U.P.A.C. Macromol. Symp., 28th, 1982, **1982**, 41.
18 R. Improta, N. Rega, C. Aleman and V. Barone, *Macromolecules*, 2001, **34**, 7550–7557.
19 F. Formaggio, M. Crisma, P. Rossi, P. Scrimin, B. Kaptein, Q. B. Broxterman, J. Kamphuis and C. Toniolo, *Chem.–Eur. J.*, 2000, **6**, 4498–4504.
20 T. S. Yokum, T. J. Gauthier, R. P. Hammer and M. L. McLaughlin, *J. Am. Chem. Soc.*, 1997, **119**, 1167–1168.
21 D. F. Kenedy, M. Crisma, C. Toniolo and B. Chapman, *Biochemistry*, 1991, **30**, 6541–6548.
22 C. Aleman, R. Roca, F. J. Luque and M. Orozco, *Proteins: Struct., Funct., Genet.*, 1997, **28**, 83–93.
23 L. Zhang and J. Herman, *J. Am. Chem. Soc.*, 1994, **116**, 11915–11921.
24 E. Schievano, A. Bisello, M. Chorev, A. Bisol, S. Mammi and E. Peggion, *J. Am. Chem. Soc.*, 2001, **123**, 2743–2751.
25 R. Burgi, X. Daura, A. Mark, M. Bellanda, S. Mammi, E. Peggion and W. van Gunsteren, *J. Pept. Res.*, 2001, **57**, 107–118.
26 J. Mahadevan, K.-H. Lee and K. Kuczera, *J. Phys. Chem. B*, 2001, **105**, 1863–1876.
27 S. Grimme, J. Antony, S. Ehrlich and H. Krieg, *J. Chem. Phys.*, 2010, **132**, 154104.
28 E. Stendardo, A. Pedone, P. Cimino, C. M. Menziani, O. Crescenzi and V. Barone, *Phys. Chem. Chem. Phys.*, 2010, **12**, 11697–11709.
29 S. Grubisic, G. Brancato, A. Pedone and V. Barone, *Phys. Chem. Chem. Phys.*, 2012, **14**, 15308–15320.
30 F. Lipparini and V. Barone, *J. Chem. Theory Comput.*, 2011, **7**, 3711–3724.
31 M. J. Frisch, G. W. Trucks, H. B. Schlegel, G. E. Scuseria, M. A. Robb, J. R. Cheeseman, G. Scalmani, V. Barone, B. Mennucci, G. A. Petersson, H. Nakatsuji, M. Caricato, X. Li, H. P. Hratchian, A. F. Izmaylov, J. Bloino, G. Zheng, J. L. Sonnenberg, M. Hada, M. Ehara, K. Toyota, R. Fukuda,

J. Hasegawa, M. Ishida, T. Nakajima, Y. Honda, O. Kitao, H. Nakai, T. Vreven, J. A. Montgomery Jr., J. E. Peralta, F. Ogliaro, M. Bearpark, J. J. Heyd, E. Brothers, K. N. Kudin, V. N. Staroverov, R. Kobayashi, J. Normand, K. Raghavachari, A. Rendell, J. C. Burant, S. S. Iyengar, J. Tomasi, M. Cossi, N. Rega, N. J. Millam, M. Klene, J. E. Knox, J. B. Cross, V. Bakken, C. Adamo, J. Jaramillo, R. Gomperts, R. E. Stratmann, O. Yazyev, A. J. Austin, R. Cammi, C. Pomelli, J. W. Ochterski, R. L. Martin, K. Morokuma, V. G. Zakrzewski, G. A. Voth, P. Salvador, J. J. Dannenberg, S. Dapprich, A. D. Daniels, Ö. Farkas, J. B. Foresman, J. V. Ortiz, J. Cioslowski and D. J. Fox, *Gaussian09*, Gaussian, Inc., Wallingford, CT, 2009.

32 (*a*) V. Barone and P. Cimino, *Chem. Phys. Lett.*, 2008, **454**, 139–143; (*b*) http://dreams.sns.it.

33 M. Marianski, A. Asensio and J. J. Dannenberg, *J. Chem. Phys.*, 2012, **137**, 044109.

34 V. Hornak, R. Abel, A. Okur, B. Strockbine, A. Roitberg and C. Simmerling, *Proteins: Struct., Funct., Bioinf.*, 2006, **65**, 712–725.

35 D. A. Case, T. A. Darden, T. E. Cheatham III, C. L. Simmerling, J. Wang, R. E. Duke, R. Luo, R. C. Walker, W. Zhang, K. M. Merz, B. Roberts, S. Hayik, A. Roitberg, G. Seabra, J. Swails, A. W. Goetz, I. Kolossváry, K. F. Wong, F. Paesani, J. Vanicek, R. M. Wolf, J. Liu, X. Wu, S. R. Brozell, T. Steinbrecher, H. Gohlke, Q. Cai, X. Ye, J. Wang, M.-J. Hsieh, G. Cui, D. R. Roe, D. H. Mathews, M. G. Seetin, R. Salomon-Ferrer, C. Sagui, V. Babin, T. Luchko, S. Gusarov, A. Kovalenko and P. A. Kollman, *AMBER 12*, University of California, San Francisco, 2012.

36 W. L. Jorgensen, J. Chandrasekhar, J. D. Madura, R. W. Impey and M. L. Klein, *J. Chem. Phys.*, 1983, **79**, 926–935.

37 T. A. Darden, D. York and L. Pedersen, *J. Chem. Phys.*, 1993, **98**, 10089–10092.

38 U. Essmann, L. Perera, M. L. Berkowitz, T. A. Darden, H. Lee and L. Pedersen, *J. Chem. Phys.*, 1995, **103**, 8577–8593.

39 J.-P. Ryckaert, G. Ciccotti and H. J. C. Berendsen, *J. Comput. Phys.*, 1977, **23**, 327–341.

40 J. L. Pascual-Ahuir, E. Silla, J. Tomasi and R. J. Bonaccorsi, *J. Comput. Chem.*, 1987, **8**, 778–787.

41 V. Barone, M. Cossi and J. Tomasi, *J. Chem. Phys.*, 1997, **107**, 3210–3221.

42 R. A. Pierotti, *Chem. Rev.*, 1976, **76**, 717–726.

43 F. M. Floris and J. Tomasi, *J. Comput. Chem.*, 1989, **10**, 616–627.

44 J. Tomasi, B. Mennucci and R. Cammi, *Chem. Rev.*, 2005, **105**, 2999–3093.

45 A. Benedetti, B. Di Blasio, V. Pavone, C. Pedone, C. Toniolo and M. Crisma, *Biopolymers*, 1992, **32**, 453–456.

46 C. Toniolo and E. Benedetti, in *Molecular Conformation and Biological Interactions: G. N. Ramachandran festschrift*, ed. P. Balaram and S. Ramaeseshan, Indian Institute of Science, 1991.

47 J. J. Smith, K. A. Bolin, H. Schwalbe, M. W. MacArthur, J. A. Thornton and C. M. Dobson, *J. Mol. Biol.*, 1996, **255**, 494–506.

48 I. Dannecker-Dörig, A. Linden and H. Heimgartner, *Helv. Chim. Acta*, 2011, **94**, 993–1011.

49 S. Carlotto, P. Cimino, M. Zerbetto, L. Franco, C. Corvaja, M. Crisma, F. Formaggio, C. Toniolo, A. Polimeno and V. Barone, *J. Am. Chem. Soc.*, 2007, **129**, 11248–11258.

50 D. Cremer and J. A. Pople, *J. Am. Chem. Soc.*, 1975, **97**, 1354–1358.